

Simulation of solar cell losses depending on cell design

A study of CIGS solar cells at Solarion AG

Master of Science Thesis in Applied Physics

Kajsa Sols

Department of Applied Physics
CHALMERS UNIVERSITY OF TECHNOLOGY
Göteborg, Sweden, 2010

Abstract

Solarion AG manufacture thin film solar cells from CIGS absorber material. In an effort to make the electricity production cheaper one approach is to optimise them, without increasing the production cost. In this project their cells were simulated with the finite element method. The layout and layer thicknesses of the front contact were considered as well as the back contact conductivity.

It was concluded that the transparent conductive oxide in the front contact and the opaque, highly conductive grid printed on top, should be optimised to give a maximal efficiency. Further the cells could be adjusted to low illumination intensities by decreasing the grid coverage.

Further, simulations of a highly resistive *i*-ZnO layer in the front contact indicate that; the layer can be used to stop short circuits between the front and back contact of the cell.

Acknowledgements

I want to thank all the employees at Solarion AG in Leipzig that made this thesis possible. You helped me have a great time in Leipzig.

Special thanks goes to my supervisor Stefan Puttnins and my stand in supervisor Dr Andreas Rahm for ideas, support and patient explanations.

I also like to thank my examiner professor Göran Wahnström for helping me with administrative challenges.

Nomenclature

ρ	Current density
σ	Conductivity
e	Elementary charge
FF	Fill factor
I	The output current
I_s	Saturation current
I_{ph}	Photo current
I_{SC}	Short circuit current
J	Current density
k	Boltzmann's constant
Q	Current source
R_p	Parallel resistance
R_s	Series resistance
T	Temperature
t	Time
V	Reverse bias voltage
V_{OC}	Open circuit voltage
CIGS	$\text{Cu}(\text{In}, \text{Ga})\text{Se}_2$
FEM	Finite element method
i-ZnO	Intrinsic zinc oxide
IBAD	Ion beam assisted deposition
STC	Standard test conditions

Contents

1	Introduction	1
1.1	Background	1
1.2	Purpose	2
1.3	Scope	2
1.4	Limitations	2
2	Theory	4
2.1	Physics of the solar cell	4
2.1.1	Absorption	4
2.1.2	Recombination	5
2.1.3	Charge separation	5
2.2	Thin film solar cells	5
2.2.1	CIGS solar cells	6
2.3	The real solar cell	6
2.3.1	Solarion AG CIGS solar cells	6
2.3.2	Solarion AG solar modules	7
2.3.3	Module production	7
2.3.4	Geometric properties of the front contact	7
2.4	Numerical techniques	9
2.4.1	Background	9
2.4.2	Equivalent circuit	9
2.4.3	Evaluation of IV-curve	10
2.4.4	Finite element method	12
2.5	Measurement techniques	14
2.5.1	Solar simulator	14
2.5.2	Low light conditions	14
3	Method	15
3.1	Simulation models	15
3.1.1	2D model of the cell layout	15
3.1.2	2D Cross section of the front contact	17
3.2	Experimental confirmation	18
3.2.1	Comparison between experiment and simulations	18
3.2.2	Test with different number of connectors	18

4	Results	20
4.1	Simulation results	20
4.1.1	General results	20
4.1.2	Optimisation of the front contact	21
4.1.3	i-ZnO layer thickness and the effect on shunts	23
4.2	Experimental confirmation	25
5	Discussion	29
5.1	Optimisations done with the layout model	29
5.1.1	Balancing conductivity and absorption	29
5.1.2	Decreasing illumination intensity	30
5.2	Optimisations done with the cross section model	30
5.2.1	Passivising shunts	30
5.2.2	Localization of shunts	30
5.3	Reliability of the results	31
5.3.1	2D model of cell layout	31
5.3.2	Evaluation of cross section model	32
6	Conclusion and outlook	33

Chapter 1

Introduction

The report describe results of simulations and experiments done at Solarion AG in Leipzig, Germany. Before the table of contents is a nomenclature including abbreviations used. All concepts from how a solar cell works in theory to how it can be simulated are described in chapter 2. The results are presented in chapter 4 and discussed in chapter 5.

1.1 Background

New sources of energy are needed as oil supply is limited and annual world consumption keep increasing. Solar power have many advantages that could make it one of the most important energy sources of the future. The influx of solar power at earth level is 162000 TW [1] while the annual energy consumption in the world was 130000 TWh in 2008 [2]. Each hour enough solar energy to sustain the global population for a year reach the earth's surface! However, this potential is still not utilised on a large scale.

The Swedish government has decided that renewable energy sources should contribute more than 50 % of the energy consumed by 2020. The Minister for Enterprise and Energy, Maud Olofsson, have stated that the goal will be reached with investments mainly in wind power and bio energy [3].

Support for solar power installation are mainly focused on smaller systems, giving a maximum grant of 2 MSKR on systems installed before December of 2011 [4].

In Germany the government plan to increase the production from renewable energy sources as well, the goal is 30 % of consumption which is almost double from the current 16 %. However, the German government has chosen another subsidising approach.

Starting in 1999 all PV produced electricity fed into the national grid has a feed-in tariff guaranteed by the government [5]. The guarantee is valid for twenty years and decrease with a set percentage each year. By supporting large scale solar power installation it becomes viable compared with other energy sources. This lead to the highest installed PV capacity in the world until 2008 [6].

The feed-in tariff has also caused some problems for the solar industry in Germany. A large and quick increase in demand lead to over-establishment and subsequent drop in solar panel prices. When the government recently decided to speed up the drop of guaranteed compensation it was feared that some companies will fail [5].

A direct comparison between the two countries are not fair as the basic conditions differ. Compared to Germany the annual power output is lower, the annual consumption pattern means large consumption in the winter when the solar influx is sparse, and the electricity prices are lower.

Still previous experiences from Sweden and Germany give clues about how to make photovoltaics a viable energy source in the future. At the moment the obstacle to a large scale break through seems to be the high price. The example from Germany show that this is surmountable with decreasing subsidies while solar panel prices are improved.

To decrease the price further there are two basic approaches. One is to make the production and mounting of the cells cheaper, decreasing the turnkey cost. Another possibility is to make the cell more efficient without making them more expensive. Simulations can help by optimising parameters in the cell without increasing the production cost.

1.2 Purpose

In this project the output of CIGS, $\text{Cu}(\text{In,Ga})\text{Se}_2$, solar cells have been investigated through simulations. Factors considered have been the design of the cell, specifically the layout of the front contact and layer thicknesses. Experimental values are used as input transmission and conductivity values; and to confirm simulation results. The goal is to use the data to investigate behaviors and optimise parameters. This should give ideas for further experiments.

1.3 Scope

The investigated parameters are related to design of the back and front contact of a solar cell:

- Thickness of the ZnO:Al layer and the effect on the optimal grid finger spacing.
- Thickness of the i-ZnO layer and how it influence shunts.
- The importance of the back contact conductivity.
- How solar cells can be adjusted to give high efficiency at illuminations below Standard Test Condition (STC).

1.4 Limitations

The calculations are demanding and therefore all models have been simplified to 2D.

To approximate the behavior of the absorber material I have used the one-diode model. In some cases I have ignored all series resistance through the solar cells. All contact resistances in interfaces have also been ignored.

The importance of grain boundaries in real CIGS solar cells have been investigated by e.g. Taretto et al. [7]; but my simulations assume homogeneous materials apart from shunt effects.

It is assumed that it is possible to keep the cells at constant temperatures at all time. In reality absorption, especially with a large influx of photons, will produce excess heating.

Chapter 2

Theory

In this chapter the basic physical principles behind a solar cell are explained. Thereafter comes a section describing how the theory are realised in real cells. Last comes a part about how those cells can be described mathematically and simulated.

2.1 Physics of the solar cell

Solar cells absorb energy by exciting electrons. The process differ between different types but this report focus on semiconductor type cells. A high power output from solar cells depend on high absorption and low recombination to get a lot of charge carriers. Additionally the positive and negative charges have to be separated in order to get a net current. [8].

2.1.1 Absorption

Semiconductors are defined by having gaps in the excitation spectra of the electrons [9]. Parts of the spectra without gaps are called bands. To excite an electron to another band the added energy has to be equal to or larger than the energy gap E_g [8].

At $T = 0$ K all electrons in a semiconductor will be in the lower band, it is therefore called valence band [8]. When all states in the band is occupied the electrons need a lot of energy to change state, no current will flow through the material. When energy is added some electrons can overcome the gap and jump to higher energy states. In this higher band there are lots of free states, the electrons can easily switch between them with only a small supply of energy. This allows them to flow through the material creating a current. The band is therefore called conduction band. [8]

When an electron is excited to the conduction band it will leave an empty state in the valence band. This empty state is called a hole and behaves like a positively charged particle with a negative mass. Both holes and electrons are charge carriers and together they are called an electron-hole pair. [8]

To maximize the current output as many electron-hole pairs as possible should be created. In a solar cell the most important generation process is the absorption of photons from the sun. For maximum absorption the band gap should be adjusted to the solar spectrum at earth level. [8].

A technique to increase the number of charge carriers in the material is to dope it. The doping atoms are called acceptors or donors. Acceptors have less valence electrons than are required for binding and easily pick up a fourth. This gives additional states just above the valence band states as well as more holes. Donors have more valence electrons than are required and easily give one away. Those additional states are just below the conduction band states. [8]

2.1.2 Recombination

The generation of electron-hole pairs is counteracted by recombination effects. Recombination is when an electron relaxes back to the valence band from the conduction band. To do this it has to get rid of the excess energy. [8]

In a reaction opposite to absorption the energy is given to a photon. Other possibilities require it to be transferred to phonons. Because phonons do not carry as much energy as photons it has to be divided between several phonons in a multistep process. [8]

2.1.3 Charge separation

To get a net current and avoid recombination it is necessary to separate the electron-hole pairs and force the particles in different directions. In a CIGS solar cell it is done by placing the absorber material between a n-doped material and a p-doped material forming a heterojunction.

The n-doped material has a larger band gap than the absorber. It is chosen so that it creates a discontinuity in the energy levels of the valence band but not in the conduction band. As a result electrons can not flow in this direction, while holes easily get through. [8]

Correspondingly there is a band gap in the conduction band between the p-doped material and the absorber keeping the electrons out.

With contacts connected to the p-doped and n-doped materials respectively the charge carriers can flow out of the cell forming a current. The current is created by an invisibly small gradient in the electrochemical potential for holes, ϵ_{FV} , and electrons, ϵ_{FC} . [8].

2.2 Thin film solar cells

Thin films are not defined by their thickness but by how they are deposited [10]. A thin film is self-assembled by nucleation and growth processes on the molecular level [10]. The assembly technique gives the films exotic properties such as the possibility for graded junctions, passivated surfaces and creation of different types of junctions [10].

Several different materials have been tested for thin film solar cells but the most common is CIGS, CdTe and a-Si:H [10]. The most popular photovoltaics

overall is multicrystalline Si, but thin films cost only about half as much to produce [11]. The cheapest thin film technology is CdTe solar cells, giving energy prices competitive with California peak prices [11]. There are however some concern about the availability of Te for large scale production [11].

2.2.1 CIGS solar cells

CIGS thin film solar cells could be a low-cost alternative for energy production [12]. A CIGS mini cell has reached an efficiency of 20.1 % in confirmed measurements [13]. Commercially produced modules has reached an efficiency of 13 % and better cells and production techniques are being developed [12].

Advantages of CIGS is the low production cost [11] and the high efficiency compared with other thin film techniques [13]. A concern is the limited availability of minerals, especially Indium that can no be easily replaced [11]. Further optimisation and decreased layer thicknesses is desirable [11].

2.3 The real solar cell

2.3.1 Solarion AG CIGS solar cells

Solarion AG manufacture thin film (CIGS) flexible solar cells. The process used is a proprietary Ion Beam Assisted Deposition (IBAD) technique. Thin films are manufactured by stimulating self-assembly between molecules. By using kinetic energy of ions to induce reactions layers can be formed at a lower temperature than with other deposition techniques.

The low temperature allows the use of Polyimide foil as a substrate for the process. Polyimide will pyrolyse at temperatures above 450 – 550 °C, compared with a glass substrate that can sustain temperatures up to 650 °C.

The foil is flexible and can therefore be used in a roll-to-roll process were the cells are made continuously. The foil is fed around rolls and the layers are deposited one by one.

The first layer is the back contact, made of molybdenum sputtered 1 – 2 µm thick. On top of that goes a 1.5 – 2 µm CIGS absorber layer. It is followed by a 40 – 80 nm layer of CdS deposited in a chemical bath.

The front contact is made of 40 – 80 nm of intrinsic ZnO, i-ZnO, followed by 200 – 800 nm aluminum doped ZnO, ZnO:Al. The two ZnO layers are sometimes referred to as transparent conducting oxide, or TCO, layer.

The name describes the relevant properties for the front contact. It has to transmit photons to the absorber, and at the same time conduct the charge carriers out of the cell. The dual functions contradict each other as a thicker layer gives better conductivity but decreased transmission. To make a thinner layer possible a high conductivity grid is printed on top of the cell. More about the grid in section 2.3.4.

A back layer a needle is used to separate a stripe of the cell from the front contact and absorber layer. The stripe is used as a contact point to the Mo layer. Finally the cells are separated from each other. In figure 2.1 is a schematic of a Solarion AB solar cell.

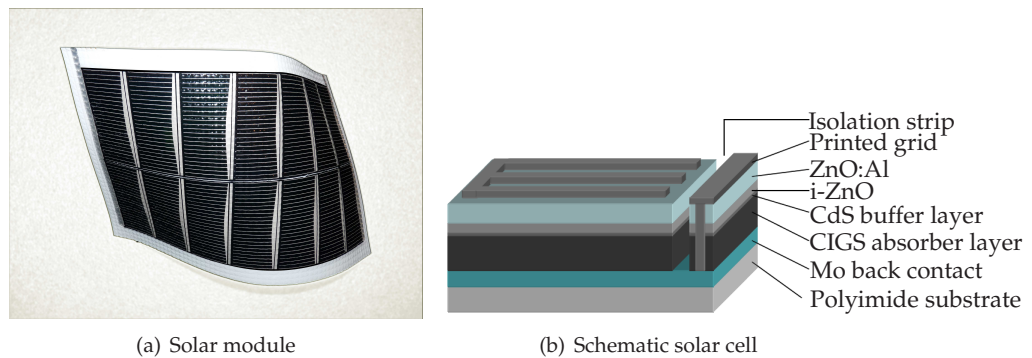


Figure 2.1: To the left a Solarion AG solar module. To the left is a schematic of a Solarion solar cell, courtesy of Zachmann [14].

2.3.2 Solarion AG solar modules

2.3.3 Module production

Solarion AG solar modules

The modules produced by Solarion AG are made in Dresden. The cells are attached to either a glass or a plastic substrate. They are placed by sucking them from the polyimide foil and then releasing them on the right spot. To make them stick they are heated and pressed to the substrate. The cells are connected by applying silver paste between the front contact of one cell to the back contact of the next. Module bus bars of copper are glued onto the the outermost cells.

When the module are dry the edges are surrounded by butyl-rubber. The module bus bars are exited through a hole in the substrate and are also surrounded by rubber. On top of the cell some embedding material is put and rigid modules are sealed off with glass rectangles while plastic are used on the flexible modules. To make them airtight they are heated until the rubber cover up all possible holes.

2.3.4 Geometric properties of the front contact

Shunt paths

If the absorber layer coverage is incomplete or have faults there is a risk for short circuits between front contact and back contact. The short circuit paths are called shunts. As they cause voltage drops and prevent charge separation it is desirable to limit their impact on the cell, if they can not be completely avoided. To mitigate the impact is called to passivate the shunt.

Virtuani et al. tested CIGS cells with different copper content in the absorber in an effort to find the reason for shunts and how to passivate them. Lowering copper content lead to an increased resistance in the cell, but also lowered the impact of the shunt. Virtuani et al. hypothesize that the shunts can be passivated because they are surrounded by absorber material. That

suggest in turn that the shunts are highly localized with a high recombination rate, rather than big but with low recombination rate. [15]

Front contact layers

The front contact of the CIGS cells are made of a thin layer of i-ZnO and a thicker layer of ZnO:Al. The i-ZnO has a resistivity of $> 10^8 \Omega/\square$ while ZnO:Al resistivity is only $> 10^1 \Omega/\square$.

To have a thick i-ZnO layer do increase the series resistance in the cell, but experiments prove that it has a positive effect on the cell performance [16]. Rau and Schmidt [17] speculates that it is because the cells include shunts. The i-ZnO layer can help to passivate them and give a more homogeneous potential distribution.

Ishizukaa et al. experimented with different i-ZnO layer thicknesses and found an optimal of 70 nm [16]. They suggested that one reason for inhomogeneities was that the CdS layer does not cover the CIGS layer completely.

An interesting effect is the possible diffusion of Al from the ZnO:Al layer into the i-ZnO layer. It should give a slightly lower resistivity that might be beneficial for the cell. However, in a thick i-ZnO layer it would only have a marginal effect [16].

To avoid voltage drops the conductivity in the ZnO:Al layer should be as high as possible. Voltage drops cause different parts of the cell to have different potential, making it impossible to get the same effect in the whole cell.

Conductivity is increased by increasing the layer thickness and printing a silver grid on top of ZnO:Al. The disadvantage is that a thicker layer lead to worse transparency, meaning fewer photons in the absorber material. These effects have to be balanced in order to get a good efficiency cell.

Grid layout

The grid is constructed with a bus bar along the long side of the cell with fingers reaching into it, figure 2.1. It has a much lower resistivity than ZnO:Al but is not transparent.

When designing the layout of the grid there are some important factors to consider. The resistances of the grid and of the front contact material determines if the charge carriers can reach the connectors of the cell. A better grid coverage give better conductivity, but on the other hand it will reflect all photons. [18].

The reflection is called shading as part of the absorber layer will be shaded from the sun. A simple assumption is that the shading loss will be proportional to the ratio of the cell covered by grid.

In reality the cells are encapsulated in a protecting material and the photons reflected by the grid fingers are sometimes deflected again. Stuckings et al. [18] calculated the factual photon loss with glass encapsulated cells and concluded that it was proportional to one third of the covered area.

2.4 Numerical techniques

When simulating solar cell it is desirable to describe them as accurately as possible. Unfortunately exact solutions often demand unrealistic amount of computing power. The only possibility is to simplify in a way that still give valuable information.

2.4.1 Background

The simplest possible model of a solar cell is to consider it as a 0D device with all processes described in one function. Different processes are described by electronic components. 0D models is further described in section 2.4.2.

To simulate parameters inside the cell and between different cells in an array the one-diode model have been extended to 1D and 2D by several authors. Using equivalent circuits simulations can be done in e.g. SPICE. The models are mainly used to investigate mismatched performance in between the cells, and how that effect the total power output [19–28]. Koishiyev et al. and Grabotz et al. also developed a 2D model, using several one-diode functions to describe different parts of a cell [29,30]

Additionally there is a couple of programs to specifically simulate solar cells. SCAPS and AFORS-HET simulate a cross section of a cell with the possibility to choose material parameters and doping levels. Both are 1D models so it is impossible to simulate cell layout with any of them. [31,32]

Malm and Edoff have worked with the finite element method (FEM) and developed several models. In 2D they have developed a cross section model where the generation and recombination rates are specified and the current flows are simulated. They have also made a model that are able to simulate the front contact including a grid finger in 3D. [33,34]

Another FEM model was developed by Brendel, it simulates thick silicone solar cells [35]. To specifically describe Si the experimentally determined absorption and recombination rate is used as input.

2.4.2 Equivalent circuit

Behaviour of a solar cell can be described by different electronic components. Each element describe characteristics of the solar cell. An example is the circuit in figure 2.2, which is a two-diode model. The voltage contacts are connected to the front contact and back contact of the cell.

The current source is used to describe absorption in the absorber layer creating electron-hole pairs, section 2.1.1. When illuminated the electron-hole pairs will give a current I_{ph} .

Parallel to the current source is two diodes. They represent the different recombination effects from section 2.1.2. In the report an even simpler model using only on-diode is used.

The parallel resistance, R_p , is also parallel to the absorption and recombination as the name suggests. It describes shunt paths in the material, section 2.3.4.

Finally the series resistance, R_s is a collective term for all material resistances in the cell and in interfaces.

Applying Kirchhoff's current law on the circuit and using the Shockley equation result in equation 2.1 [36]:

$$I = -I_{ph} + I_s \left(\exp \left(\frac{e(V - IR_s)}{nkT} \right) - 1 \right) + \frac{V - IR_s}{R_p} \quad (2.1)$$

The model can be used to calculate the performance of a cell by doing a voltage sweep and extracting the current. Using typical parameters it gives an IV-curve like in figure 2.2 for one cell. As $P = VI$ the power is easily calculated, it is plotted in the same figure. Current in the fourth quadrant give positive power output. In the dark the current at $V = 0$ is zero.

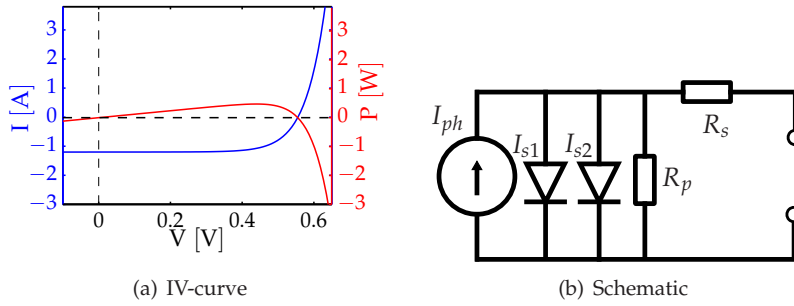


Figure 2.2: a) IV-curve and power output of a typical cell. b) An equivalent circuit called the two-diode model. Each component describe characteristics of the solar cell.

2.4.3 Evaluation of IV-curve

A highly efficient solar cell has a large power output compared to the illumination intensity. To evaluate how well a cell functions, and what parameters that could be improved; it is possible to study the parameters in the one-diode model, section 2.1, and the effect they have on the power output.

Fill factor

The theoretical maximum output is that of a cell without any resistance or recombination effects. Such a cell would be operating at the open circuit voltage, V_{oc} , and still put through the short circuit current, I_{ph} .

The maximum obtainable power is easily calculated from an IV-curve measurement as $P = VI$. Figure 2.4.2 includes the power characteristics for the simulated cell. When operating at the optimal voltage V_{MP} the cell is said to be at its maximum power point.

To estimate losses in the cell the fill factor (FF) is calculated. It is defined as

the maximum obtainable power divided by the maximum theoretical power.

$$FF = \frac{I_{mp} V_{mp}}{I_{sc} V_{oc}} \quad (2.2)$$

FF will always be less than 1 in a real cell but can reach 0.8 for high quality cells [13].

One-diode model parameters

The parameters of the one diode model, equation 2.1, is T , R_p , R_s , n , I_s and I_{ph} . Assuming that the cell operates at room temperature leaves R_p , R_s , n , I_s and I_{ph} .

All electron-hole pairs created give the maximum current I_{ph} . Comparing the parameter with illumination tell how good the cells is at absorbing photons. Figure 2.3 show the effect on the IV-curve of changing I_{ph} and I_s

I_s is the recombination constant. When it is high the recombination is equal to absorption at a low V . Lowering it means that the open circuit voltage increase.

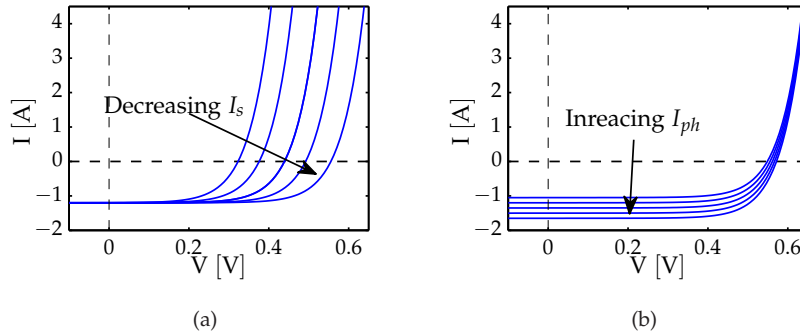


Figure 2.3: Influence of current parameters on the IV-curve. a) Photo current describes the absorption of the cell. b) A smaller saturation current means that the give a higher open circuit voltage.

The parallel resistance, R_p , defines the possibility for the current to bypass the CIGS layer and recombine. It is a linear effect depending on voltage, variations shown in figure 2.4.

A high series resistance in the cell cause large voltage drops in the cell, in turn causing parts of the cell to work outside of the maximum power point. If R_s is within normal ranges the result is mainly visible at high voltages.

In figure 2.5 the effect of a non-ideal diode is shown.

For simplicity the characteristics of a cell can be described by I_{ph} , V_{oc} and FF . I_{ph} and V_{oc} is the maximum capability of the cell while FF describe how well the cell work in reality.

Efficiency of a solar cell is defined as output power divided by illumination power on the solar cell. In the simulations there parameters are chosen to represent a certain illumination intensity. The calculated efficiency should therefore be viewed as that of an envisaged cell under a specific illumination.

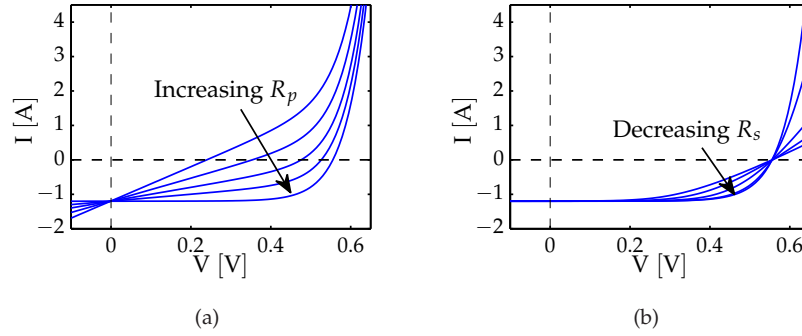


Figure 2.4: Influence of resistance parameters on the IV-curve. a) High parallel resistance means few shunts. b) High series resistance cause voltage drops in the cell worsening the performance.

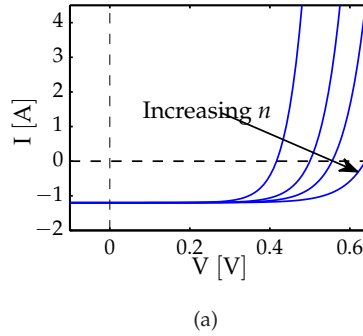


Figure 2.5: Influence of diode ideality factor on the IV-curve.

2.4.4 Finite element method

The Finite element method (FEM) is a method to simplify, and usually to decrease, computation time. It translates a continuous problem into a discrete, numerically solvable problem [37]. It is used to solve PDEs on complicated geometries or with complicated boundary conditions.

FEM divides a geometric domain into discrete elements. On each element a particular form of the solving function is assumed [38]. By requiring continuity on element boundaries the problem can be translated into a sparse matrix. It can be solved with numerical methods [38].

To solve a problem with FEM a PDE, boundary conditions, shape and spacing of the elements as well, as the form of the assumed solution need to be specified.

PDE formulation on a solar cell

The creation and flow of electric charge is described by the continuity eq 2.3.

$$\nabla J(\mathbf{R}, t) = -\frac{\partial \rho(\mathbf{R}, t)}{\partial t} \quad (2.3)$$

Using ohms law $J = \sigma E$ and the definition $E = -\nabla V$ we get the PDE, eq [34]:

$$\nabla(\sigma \nabla V(\mathbf{R}, t)) = \frac{\partial \rho(\mathbf{R}, t)}{\partial t} \quad (2.4)$$

$\frac{\partial \rho}{\partial t} = Q$ is a current source, in a solar cells it can be used to describe the absorption of photons and different recombination mechanisms.

The possible boundary conditions are Neumann boundary conditions eq 2.5, eq 2.6, Dirichlet boundary conditions eq 2.7, eq 2.8, and imposed jumps in the internal current eq 2.9.

$$n \cdot J = 0 \quad (2.5)$$

$$n \cdot J = J_s \exp\left(\frac{e(V - JR_s)}{nkT} - 1\right) + \frac{(V - JR_s)}{R_{sh}} - J_{ph} \quad (2.6)$$

$$V = 0 \quad (2.7)$$

$$V = V_{applied} \quad (2.8)$$

$$n \cdot (J_1 - J_2) = \sigma \Delta V \quad (2.9)$$

Eq 2.5 describes electrical insulation and is used on external boundaries and symmetry lines in the model. Eq 2.6 describes a boundary where the charge carriers are created outside of the defined geometry and are flowing in. Eq 2.8 describe a voltage source applied the back contact of the cell to get an IV-curve. Eq 2.7 is the corresponding grounded contact.

It is equation 2.4, which is called Poisson's equation, that is solved for using the finite element method [34, 37].

Weak constraints The results of the simulations are the potential distribution and the current density throughout the cell. To get the IV-curve the current density have to be integrated over a contact boundary.

In the standard FEM formulation the fluxes are inaccurate making it impossible to calculate correct currents. The reason is that they are computed outside of the solution matrix. This can be solved by using weak constraints. In the weak form the PDE is rewritten using Lagrange multipliers, λ . They are solved as a part of the solution matrix together with other unknowns. Solving the electrostatic Poisson's equation λ represent the current density and integrating them over the connectors give the total current. [34]

$$I = \int \lambda_1 dS \quad (2.10)$$

The details fall outside the scope of this thesis but can be found in books about the finite element method, e.g. Johnson [37].

COMSOL

COMSOL is a commercial software for multiphysics simulations with the finite element method. It can be used by itself or as a MATLAB toolbox. Models are either drawn in CAD or defined by scripting. It has predefined applications for several PDEs including Poisson's equation 2.4. [39]

2.5 Measurement techniques

2.5.1 Solar simulator

To measure the IV-curve of a real solar cell the current is measured while keeping a specified voltage difference between the back contact and the front contact. A sweep is done over a set of voltages giving an IV curve very similar to the simulated in figure 2.2. By fitting a one-diode model curve to the measured values parameters can be extracted and then used to evaluate the cell.

During the measurement the flexible cells are placed on a suction table, in order to stay flat, underneath a lamp that conforms to standard test conditions (STC). At STC the spectrum is 1.5 AM and 1000 W [1]. The table will keep the cell flat and also cool it so the temperature is constant at 25 °C.

On top of the cell a measuring device is placed with 8 pins on each of the bus bars. The pins are connected collectively to a multimeter which in turn is connected to a computer. The pins are kept at a constant voltage for each measurement. It has been noted when doing the measurements that the output increase if the device is pressed down on the cell.

2.5.2 Low light conditions

Official measurements of solar cells and record cells are measured at STC.

In common applications the power is much lower part of, or all of the time. Examples are solar cells when it is cloudy, in the morning and solar cells integrated in electronic products and clothing. Therefore it is interesting to test how the influence of certain parameters change in different light conditions.

Chapter 3

Method

This chapter describe the models used for the simulations and the experiments done to collect data and confirm the models. First section 3.2 explain simulation models used. Thereafter section 3.1 describe some experiments done to test the accuracy of the simulations.

3.1 Simulation models

The general problem formulation is in section 2.4.4. In this part the boundary conditions, conductivities and current sources used are detailed.

3.1.1 2D model of the cell layout

The model describe the layout of the cell as seen from the front, figure 3.2(a). It include grid fingers, front contact and connectors.

The connectors are situated on the bus bar and grounded with boundary condition 2.7. Remaining internal boundaries were calculated with a continuous boundary condition.

External boundaries are assumed to be electrically insulated, $nJ = 0$, because they are surrounded by air, a good insulator. The same boundary condition can also be used at all symmetry lines, as the net current through them will be zero. By using this the simulation could be limited to a quarter of a standard size cell.

Electron-hole generation is approximated with a distributed one-diode model 2.1. It was assumed that the main series resistance was in the front contact in the model plane. Using this approximation the series resistance in the one-diode model could be set to zero; the function becomes explicit instead of implicit. It is also assumed that the material is homogeneous in the cell. The absorption is then equal in the whole cell except underneath the grid fingers, because they are opaque.

Recombination and the influence of the parallel resistance depend on the potential difference between back and front contact. Assuming a perfectly conducting back contact the back contact potential, V_{back} , is homogeneous. The

difference is then calculated as $\Delta V = V_{back} - V(x, y)$ in each point.

The transmission and conductivity of the front contact at different ZnO:Al thicknesses were measured on Solarion AG cells at STC. A linear fit was made to the photo current and a quadratic fit to the sheet resistance. Measurements and fitted curves are depicted in figure 3.1. The fitted functions were used to describe a front contact with different thicknesses. The actual ZnO:Al layer thickness is an industrial secret so the scale is normalised in this report.

In addition to the photo current dependence on front contact thickness it was assumed that it is linearly dependent on the illumination intensity.

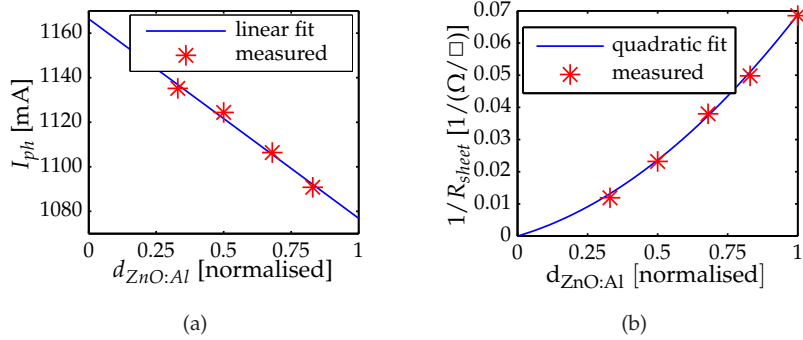


Figure 3.1: Transmission and conductivity were measured depending on ZnO:Al layer thickness. Figures show measurements and fitted functions. a) Change in photo current. b) Change in sheet resistance.

Conductivity of the grid fingers were taken from measurements done at Solarion AG on typical cells.

The total current is integrated over the contacts on the bus bar.

COMSOL has an interface to MATLAB that are used to control the simulations and vary different parameters. In the layout model width, length, the number of fingers, the number of connectors, and σ is varied. The computations were performed on C3SE computing resources.

Finite conduction in back contact

To test the assumption that the resistivity in the back contact is negligible compared to that of the front contact, a model with finite back contact conductivity was created.

COMSOL has the ability to simulate several PDE:s simultaneously and couple the solutions. Using one PDE to solve on the back contact and one to solve on the front contact the solutions were coupled in the one-diode model. The potential difference in this case were $\Delta V = V_{back}(x, y) - V(x, y)$.

Parameter sweeps

The 2D layout model were used to simulate four different parameters. With infinite back contact conductivity finger spacing, ZnO:Al layer thickness, and illumination were changed.

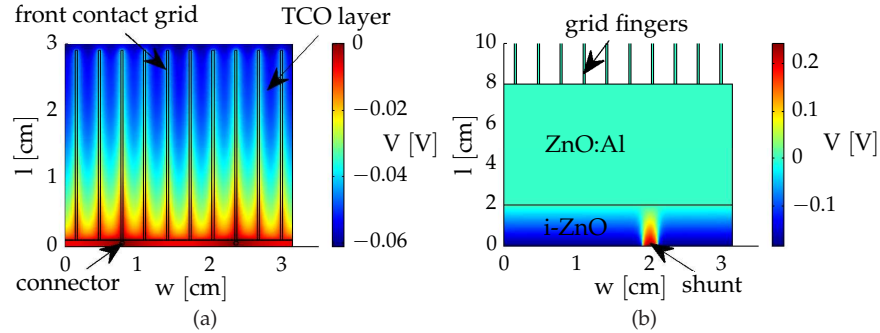


Figure 3.2: The two models used for fem simulations

With finite back contact conductivity the conductivity was varied.

3.1.2 2D Cross section of the front contact

A cross section model that includes the two ZnO layers and grid fingers, figure 3.2.

The two layers were constructed as squares with an inward current flow at the bottom of the i-ZnO. On top of the ZnO:Al layer is the grid fingers. It is assumed that the grid is perfectly conducting.

The current source were included in the boundary condition at the bottom of the i-ZnO layer. Similarly to the layout model the resistance outside of the front contact is ignored giving an explicit form of the one-diode model.

Apart from the bottom boundary all outside boundaries are described as electrically insulated, and all inside boundaries as continuous.

In accordance with the model outlined by Malm and Edoff [33] the layers were extended by a factor of 100 in the y-direction to improve the scaling of the mesh in COMSOL. To get the correct conductivity it was increased in the y-direction and decreased in the x-direction.

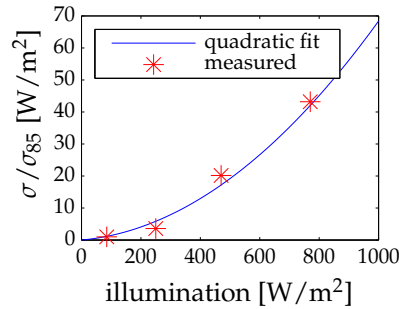
A shunt was included by having a part of the cell with parallel resistance in the order of eight times lower than in the rest of the cell. It was also assumed that there was no absorption in this part. It was characterised by how big it was in compared with the rest of the cell in percent.

Performance at low illumination intensities were simulated by assuming a linear dependence of I_{ph} and two different models for the i-ZnO conductivity. The first assumed a constant conductivity. After measurements done at Solarion AG on pure i-ZnO at different illuminations a model with illumination dependent conductivity was tried as well. Measurements and fit in figure 3.3.

Simulations

Three different simulations were done with this model.

Using measurements done at real Solarion AG solar cells as a model; attempt was made to adjust the parameters of the simulation to get the same output using the two conductivity functions.



(a)

Figure 3.3: The stars are measured values of i-ZnO conductivity while the line show a quadratic fit.

Using a 6 % shunt with a parallel resistance of 0.1Ω a sweep over different illuminations were done. The optimal i-ZnO layer thickness were calculated at each illumination. Both conductivity models were used.

With a constant parallel resistance the size of the shunt were varied at different i-ZnO layer thicknesses.

3.2 Experimental confirmation

The experiments and simulations explained in this chapter was made to confirm the accuracy of the simulation models. In the first test old measurements done at the company is used. The other measurements were done as part of the project.

3.2.1 Comparison between experiment and simulations

In a previous experiment at Solarion AG the performance of a solar cell was measured in a solar simulator. After that it was processed. It was confirmed that the voltage drop in the grid fingers decreased from 170 mV to 20 mV afterward. It is unknown how the processing otherwise affected the cell. The IV-curve was measured before and after, fitted to the one-diode model, and all changes in the parameters were recorded.

To test the accuracy of the 2D model a cell with the same layout as the measured cell was created. Parameters were tuned until the output was similar to that of the measured cell before processing. Thereafter the grid conductivity was increased. Parameters from measurement and simulations are recorded in section 4.2.

3.2.2 Test with different number of connectors

Five cells of good quality were chosen and their IV-curves were measured in the solar simulator, section 2.5.1. Thereafter the cell was measured with pins

isolated from the cell with isolating foil. Measurements were done with between one and eight pins in contact with the cell.

The measuring device have two rows of 8 pins located approximately 29 mm apart from center to center. Each connector was about 1 mm in diameter.

Simulations was done with the 2D front contact model including back contact 3.1.1. It was adjusted to have the right placement of connectors.

Chapter 4

Results

The results are presented in the same order as the models are described in the methods chapter. Starting of with the 2D layout model, than the 2D cross section model and at last the experimental confirmations.

4.1 Simulation results

Section 4.1.1 and section 4.1.2 include results from the 2D layout model described in section 3.1.1. The next part 4.1.3 explains the result of the 2D cross section model.

4.1.1 General results

Voltage drop and generated current

The front contact has a small voltage drop along the fingers and a large voltage drop between the fingers. Figure 4.1 shows the potential drop at the maximum power point and how the generated current depends on the potential. There is no photons transmitted through the fingers and therefore there is no absorption underneath them.

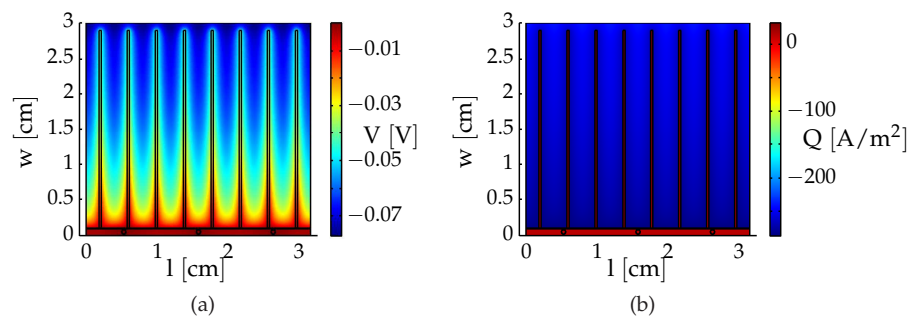


Figure 4.1: The front contact of a typical simulated cell. a) Electric potential. b) current source.

Back contact conductivity

In order to save computing time infinite back contact conductivity was assumed in most simulations. In figure 4.2 a comparison between this model and the one with finite back contact conductivity is made. The dashed line symbolise normal conductivity in Solarion solar cells.

The back contact conductivity seem to have a linear dependence on the efficiency. An infinite back contact conductivity gives about 0.4 % higher efficiency than normal conductivity.

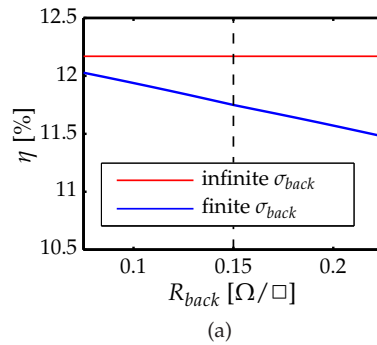


Figure 4.2: Efficiency of a solar cell with different back contact conductivity. The red line show the efficiency of a cell with perfect conductivity.

4.1.2 Optimisation of the front contact

Finger spacing

The number of fingers on the cell were varied between 4 and 30 fingers. Figure 4.3(a) show the result at a ZnO:Al thickness of 0.7 units. The efficiency has a maximum at a finger spacing of 3.2 mm. It can be noted in the figure that the resulting curve is not completely smooth.

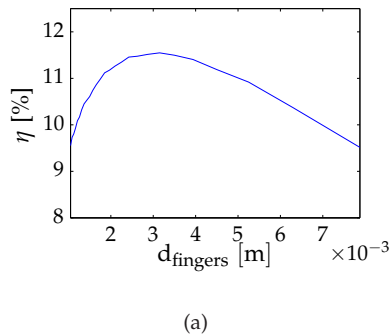


Figure 4.3: Efficiency when varying finger spacing at STC with a 0.7 units thick ZnO:Al layer.

Figures of the potential distribution in the cells show the influence of the finger spacing. With a short finger distance the voltage drop is small, while at 7.875 mm it is more than 0.15 V, figure 4.4. The voltage drop at the maximum finger distance is about 0.05 V, one third of that with four fingers, figure 4.5(a). On the other hand the photo current increases with fewer fingers, figure 4.5(b).

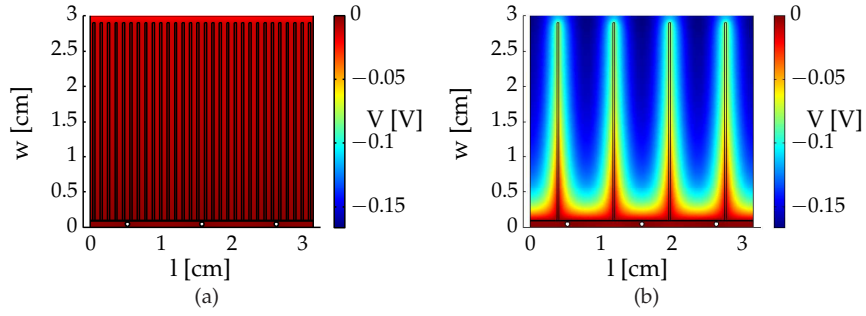


Figure 4.4: Voltage drop with very extreme finger distances a) Finger spacing 1.05 mm. b) Finger spacing 7.875 mm.

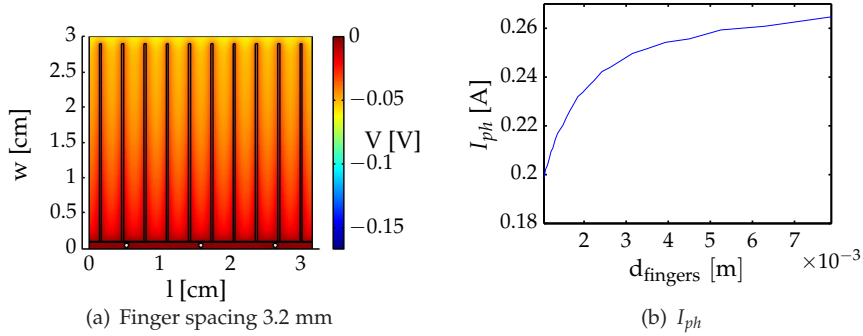


Figure 4.5: a) Voltage drop with a finger spacing near maximum efficiency. b) Photo current increase with finger spacing because of less shading.

ZnO:Al layer thickness and finger spacing

In the next simulations finger spacing and ZnO:Al layer thickness are varied simultaneously. For each thickness the optimal finger distance and the maximum efficiency with optimal spacing were calculated. To avoid influence by the local maximums, caused by the unevenness, a polynomial was fitted to the curve and the maximum was calculated from this fit.

With increasing thickness fewer fingers are needed as seen in figure 4.6(a). In figure 4.6(b) is the efficiency with optimised finger spacing at each thickness. The optimal cell has a ZnO:Al layer that is 0.4 units thick and a finger distance of 2.9 mm.

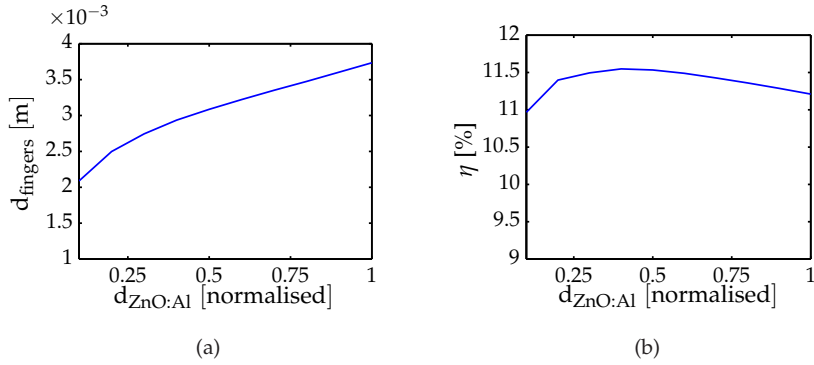


Figure 4.6: The finger distance was varied at each ZnO:Al layer thickness. b) The optimal finger distance. a) Efficiency with optimal finger spacing.

From the simulated IV-curves the parameters, as described in section 2.4.3 were extracted. As the simulations are discrete and the parameters were affected by the unevenness a polynomial was fitted to them depending on finger spacing. From this fit the parameters at the optimal finger spacing could be extracted. Some of them are plotted in figure 4.7.

The series resistance is high when the ZnO:Al layer is thin but seems to saturate at about 0.3 units when the finger distance are adjusted. The fill factor changes in the opposite way, first it increase rapidly for thin layers to thereafter saturate with a maximum at 0.5 units.

U_{oc} first increase but change very little for thicker layers. The most distinct maximum is that of I_{ph} around 0.3 – 0.4 units slightly below the most efficient cell at 0.4 nm.

Low illumination intensity

The previous simulations were done with parameters typical for measurements at STC. Other simulations were done with the photo current lowered to simulate low light conditions. In figure 4.8(a) the efficiency of a cell optimised for STC is compared with cells optimised for each illumination intensity. The adjustments, shown in figure 4.8(b), is a simultaneous decrease of $d_{ZnO:Al}$ and increase of $d_{fingers}$ at low illumination intensities. For low intensities an adjusted cell has an efficiency that is about 0.5 % better than an unadjusted cell.

In figure 4.9 the influence of the adjustments are separated. When only changing ZnO:Al thickness the change in efficiency are small compared to making no adjustments. However, adjusting only the finger spacing were almost as effective as adjusting both parameters.

4.1.3 i-ZnO layer thickness and the effect on shunts

Comparison with measurements

Two different models for the i-ZnO conductivity was used and compared to measurements of real cells. The simulation at STC were done by adjusting

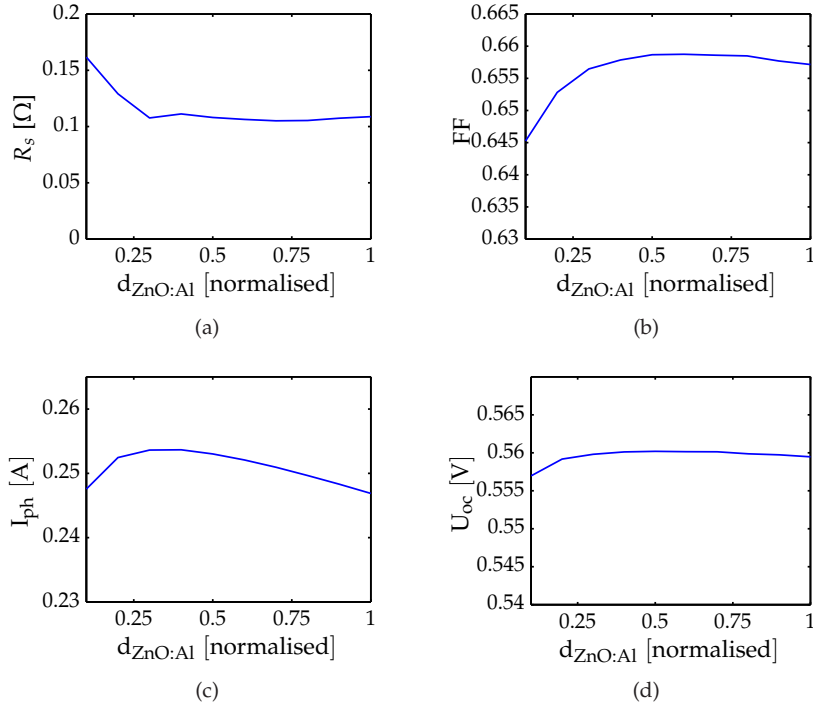


Figure 4.7: IV-curve parameters at optimal finger spacing. a) R_s , b) FF , c) I_{ph} and d) U_{oc} .

the shunt localisation, R_p , and i-ZnO conductivity. The result is similar to the experimental values but not exact, figure 4.10(a).

In figure 4.10(b) the two approaches are compared with measurements at 70 W/m^2 . Only the photo current and in one model the i-ZnO conductivity were adjusted. Neither of the simulations give results that resemble measurements.

In figure 4.11 the optimal i-ZnO thickness at each illumination is shown. It is clear that the tendencies of the two models is opposite. A decreasing conductivity at lower illumination give lower optimal thicknesses while a constant conductivity gives higher.

Localization of shunts

Using the same total shunt and photo current the localization of the shunt was changed; by changing the ratio between it and the width of the cell. The R_{sh} and the R_s of the IV-curve can be seen in figure 4.12(a). Both increases with increasing i-ZnO layer thickness.

In figure 4.12(b) is experimental values of the resistances measured on Solarion AG solar cells. The series resistance increase linearly in both experiments and simulations. Measurements show an exponential increase in parallel resistance with thicker i-ZnO layer but this behaviour was not reproduced in simulations.

It can be noted that the simulated R_{sh} dependence on the thickness increase

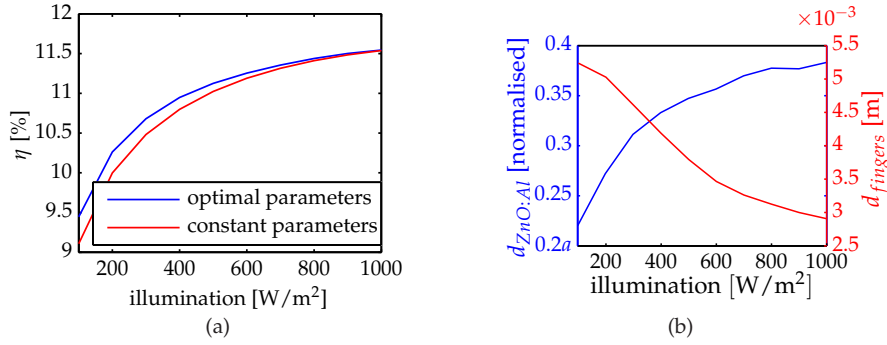


Figure 4.8: Comparison between a solar cell optimised for each illumination and a cell with constant parameters. a) Efficiency in both cases. b) Adjustment of the parameters.

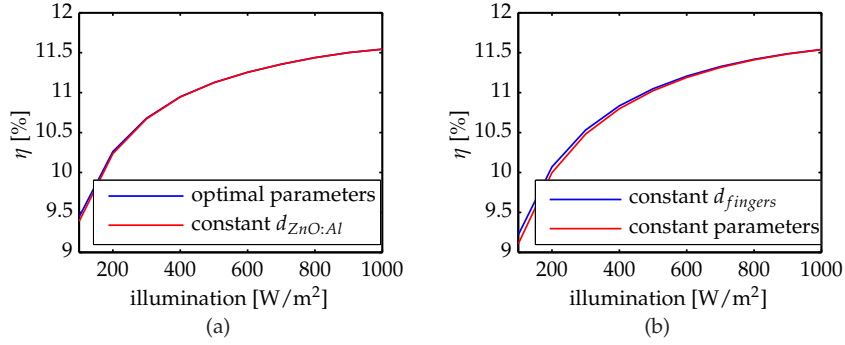


Figure 4.9: a) Optimising only finger spacing with constant $d_{ZnO:Al}$ gives an efficiency close to the optimal cell. b) Fine tuning $d_{ZnO:Al}$ compared to constant $d_{ZnO:Al}$.

with the localization of the shunt. R_s on the other hand show no dependence on localization. Unfortunately it was not possible to determine the shunt size in the real cells.

4.2 Experimental confirmation

Comparison with processed cell

Processing a real cell to improve the grid conductivity lead to the improvements to the left in table 4.1.

To make a comparison possible the parameters of a simulated cell was adjusted. The simulated results resembled the measured cell both in parameters and in voltage drop. Thereafter the grid conductivity was improved from 170 mV to 20 mV. The change lead to the improvements to the right in the table.

In both cases the efficiency increase, but in the simulations it is mainly a

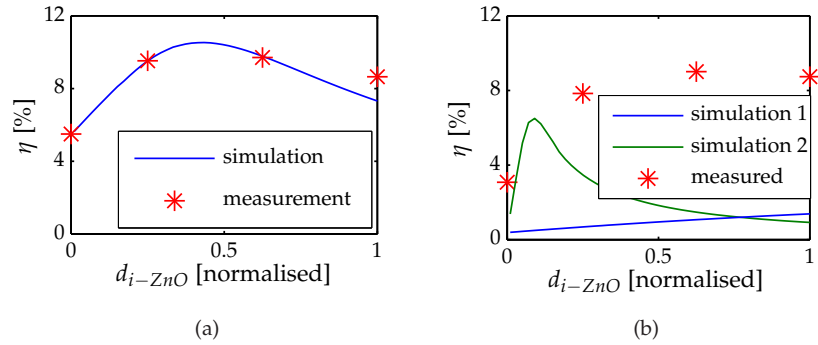


Figure 4.10: Simulated and measured efficiency of the cell at different i-ZnO thicknesses. a) At STC. b) At 70 W/m^2 with two different models for i-ZnO conductivity.

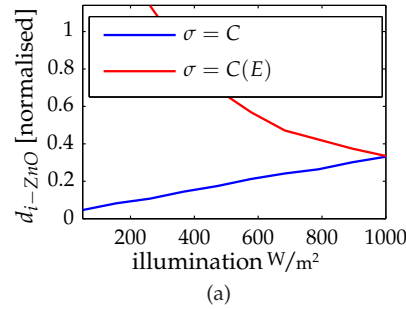


Figure 4.11: Optimal thicknesses at different illuminations. The blue line show results if the conductivity is constant. The red line with a decreasing conductivity at low illumination.

result of improved fill factor. The real cell also got an improved photo current but a slightly worse open circuit voltage. The changes in experiment and simulation are otherwise similar, with the exception of small increase in parallel resistance instead of a small decrease.

Varying the number of connectors

The results from measurement done with different number of pins were compiled. The standard deviation of the different values were calculated. The IV-curves from the simulations were fitted to an IV-curve made with a one-diode model and the parameters were calculated.

Figure 4.13 depicts the result with the lines representing the simulated values and the stars the experimental values. To make a comparison easier all values are normalised to the value with eight pins.

The open circuit voltage were constant in the simulations and almost constant in the experiment. I_{SC} , FF , and η on the other hand improved with more connector pins both in simulations and measurements. It can be noted that the

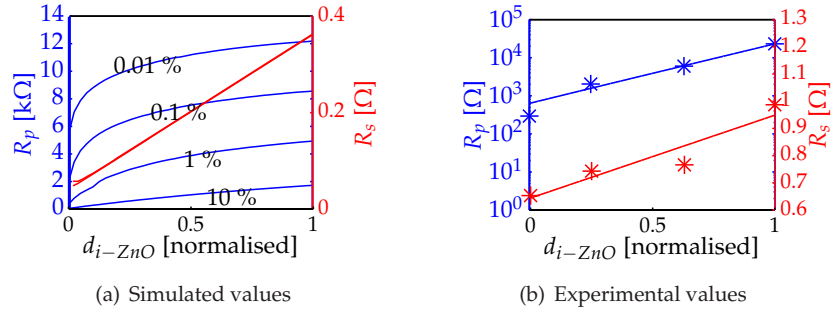


Figure 4.12: Variation in R_{sh} and R_s with increasing i-ZnO thickness. The ratio is the shunt width divided by cell width.

Table 4.1: Change in parameters when improving grid conductivity. Comparison between experiment and simulation.

	Values			
	Experiment before	Experiment after	Simulation before	Simulation after
η [%]	7.87	10.07	6.77	8.33
FF	0.48	0.57	0.48	0.59
I_{ph} [mA]	775.6	846.8	776.3	778.6
I_{sc} [mA]	772.0	843.4	771.0	777.9
I_s [mA]	3.97	0.12	2.67	0.15
V_{oc} [V]	528.6	519.2	587.8	587.8
R_s [mΩ]	97.43	71.67	76.6	13.3
R_p [Ω]	20.87	17.76	11.2	15.9
n	3.92	2.27	4.08	2.69

experimental values in general is slightly lower with few connector pins.

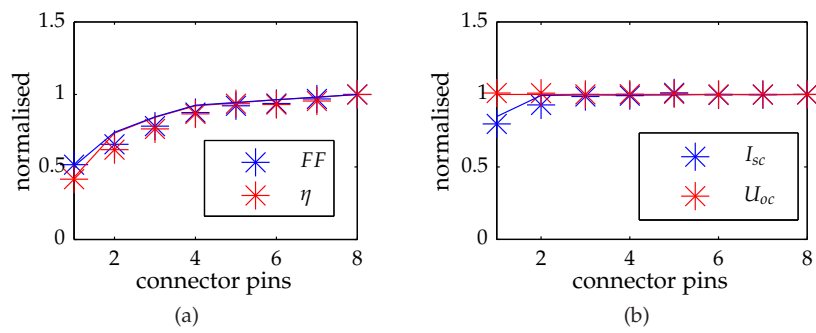


Figure 4.13: Change in parameters by varying the number of connector pins. Lines represent simulations and points are experimental values. a) Fill factor and efficiency. b) Short circuit current and open circuit voltage.

Chapter 5

Discussion

In the first parts the optimisation results of the two models and their implications are discussed. The order are the same as used in previous chapters. In the last part the reliability and limitations of the results are brought up.

5.1 Optimisations done with the layout model

5.1.1 Balancing conductivity and absorption

When varying the finger spacing an optima was found for each ZnO:Al thickness. With increasing front contact thickness the required number of fingers decreased. The result is in agreement with Stuckings et al. whom stress the importance of balancing grid and front contact conductivity, section 2.3.4. When the ZnO:Al thickness increases conductivity increase, reducing the need of grid fingers.

Stuckings et al. also claims that the encapsulation of cells will reduce the shading effect of the fingers. In this project the effect has not been considered, but if it is true it would be beneficial to decrease the finger spacing more.

Solarion AG solar cells are used for both flexible and rigid modules with different types of encapsulation. It is possible that the optimal design would change depending on the encapsulation technique. Further studies need to be to investigate if the difference is big enough to motivate different type of cells in different modules.

With optimised finger spacing the series resistance are almost constant over a threshold value, figure 4.7(a). Also the fill factor, that are influenced by the series resistance, first increase but for thicker ZnO:Al layers is almost constant. The bad fill factor at thin layers is likely an effect of the high series resistance.

The main determinant of the efficiency maxima seem to be the photo current, figure 4.7. Maximum of I_{ph} at 0.3 – 0.4 units is only slightly below the efficiency maxima at 0.4 units. The difference depend on an increase in the fill factor for thicker layers. In this range the balance between photon transmission and conductivity is the best.

5.1.2 Decreasing illumination intensity

At low illumination the photo current decreases linearly. When all other parameters constant the efficiency also decreased in the simulations, figure 4.8(a), indicating a correlation between the two. By increasing the finger distance and decreasing the ZnO:Al layer thickness cells with better behaviour at low illumination intensities can be produced, figure 4.8(b).

Both adjustments will decrease the conductivity and increase the absorption. It seems that the balance between the parameters is damaged by decreasing illumination and thereby the photo current. However, simulations indicate that it is possible to readjust the cells limiting the efficiency decrease. The results also indicate that the readjustment can be done almost solely by increasing the finger spacing.

This kind of adjustments could be valuable in solar installations outside of designated parks. Many solar modules are installed at suboptimal conditions. E.g. modules on buildings are often integrated either horizontally or vertically, even though this is not optimal from a illumination perspective. These cells will often work at illumination intensities below STC.

For modules operating at 200 W/m^2 the difference could be about 0.5 % according to simulations.

5.2 Optimisations done with the cross section model

5.2.1 Passivising shunts

Both Rau et al. and Ishizukaa et al have found that the i-ZnO layer has a positive effect at the cell and argue that it help to passivate the shunts [16,40]. The simulations also indicate that a thicker i-ZnO layer might have a positive effect when the cell is shunted.

Unfortunately neither of the two conductivity models gave an accurate description of the cell behaviour at low illumination intensities. However measurements indicated that the conductivity does increase at low illuminations, section 3.1.2. A problem with the measurements might be that they were done on pure i-ZnO. Ishizukaa et al. speculate that the aluminum from the ZnO:Al layer penetrate into the i-ZnO layer leading to a higher conductivity in the affected parts. This effect would be more prominent in thin layers causing a non-linear effect in the i-ZnO layer only when it is integrated in the cell.

5.2.2 Localization of shunts

An interesting effect where that the importance of the i-ZnO layer increased with a more localized shunt. This is in line with the reasoning by Virtuani et al., highly localized shunts can be more easily surrounded and passivated [15].

5.3 Reliability of the results

5.3.1 2D model of cell layout

Experimental verification

Two tests were done with the layout model in order to verify it. In the first it was compared with a cell processed to get improved grid conductivity. In the second simulations and measurements were done with different number of connectors.

Improving grid conductivity gave better FF , I_s , R_s , and n in both experiment and simulation. That the series resistance decreases with better conductivity is obvious. It also seems reasonable that a decreased voltage drop would make a larger part of the cell work at or near the maximum power point. That could explain the increased FF , I_s and n .

In the experiment the photo current and V_{oc} also are affected, while they are unchanged in simulations. The grid conductivity should have no effect on the absorption as they are opaque. Because no current is flowing at open circuit conditions V_{oc} should be unaffected as well. It is likely that those two changes are caused by another change in the cell that has not yet been determined. Maybe the process effect the front contact layer as well, e.g increasing the transmission.

When varying the number of connectors the tendencies of the simulated parameters are similar to the measured ones. This is true for all four parameters and indicate that the 2D layout model give a reasonable description of real cells.

One reason for the slightly lower values of experimental parameters with few pins could be the connection of the pins with the cells. Using only a few pins a bad connection between pin and cell should have a larger effect than when using many pins.

Back conductivity

A realistic back conductivity gives about 0.4 % lower efficiency of the cell compared with a infinite conductivity. The change in absolute values is not insignificant. I was not possible to use finite back contact conductivity in all simulations as the computation time increased quite a lot. Maybe it would still be possible to make some simulations to see if it effect other results as well.

Input parameters

Input parameters for the ZnO:Al simulations were mostly fitted from measurements. Without surface effects a thicker layer should give a linearly increasing sheet resistance and linearly decreasing transmission. However, as seen in figure 3.1 a linear model fitted to measured values would give a negative sheet resistance for thin layers. .

As a negative resistance would be unphysical a quadratic fit was used instead, but it is not known if this is a good description of the behaviour at low

illuminations. A reason for the measured values could be surface effects or poor coverage giving poor conductivity in the uncovered parts.

Evaluation of layout model

The 2D layout model give reasonable results that have the same tendencies as measurements done on real cells. It does however have some limitations. Because of long computation times both back contact conductivity and resistances outside of the model and in interfaces have been ignored. The comparison with the same model but finite back contact conductivity indicate that absolute values might differ with a more complete model.

Still, even if the absolute values are inexact the results can be useful. They give an indication about how cells can be improved and which parameters that are important.

5.3.2 Evaluation of cross section model

The 2D cross section model were compared with measurements done with different i-ZnO layer thicknesses and illumination intensities. The series resistance is linear in both cases while the parallel resistance is poorly described by the simulations. Neither did any of the low illumination models resemble the measured results.

As the model could not be experimentally confirmed the results should not be relied upon. Still the influence of shunt size on the possibility to passivate it is interesting. With a better model it might be possible to simulate how thick i-ZnO layers are needed for different average shunt sizes.

Chapter 6

Conclusion and outlook

According to the simulations it is beneficial to keep the ZnO:Al layer thin, under condition that the conductivity can be brought over a certain threshold without sacrificing too much absorption. To get better efficiency the finger spacing can be adjusted, using a smaller finger distance on a thin layer.

When decreasing the illumination intensity a cell optimised at STC will perform badly. By adjusting the cell the efficiency can be increased with more than 8 % at a 200 W/m^2 illumination. Adjustments can be done in both ZnO:Al layer thickness and finger spacing but the most important factor is the finger spacing.

A cell with a realistic back contact conductivity has about 0.4 % lower efficiency than a cell with infinite conductivity.

It is indicated that the possibility to passivate shunts with i-ZnO is dependent on the shunt localisation. In order to test this further the shunts and how they are localised has to be investigated. A first step could be to develop a more accurate model than the one used for simulations.

The model of the cell layout has shown the same tendencies as real cells in several measurements and have given physically reasonable results. It could be extended to simulate other parameters. Interesting things to look in to could be inhomogeneities in a cell, number of connector points, and the effect differing parameters between cells have on module output.

Bibliography

- [1] D. Ginley, M. A. Green, and R. Collins, "Solar energy conversion towards 1 terawatt," *MRS. Bulletin*, vol. 33, pp. 355–374, 2008.
- [2] "Energiläget 2009," tech. rep., Statens energimyndighet, 2009.
- [3] M. Olofsson, "Vi ska bygga 2000 nya vindkraftverk på tio år," *Dagens Nyheter*, pp. <http://www.dn.se/debatt/vi-ska-bygga-2-000-nya-vindkraftverk-pa-tio-ar-1.1054315>, 2010.
- [4] F. Nilsson, M. Brogren, and L. Palmblad, "Nytt investeringsstöd för solceller," June 2009.
- [5] J. Hällén, "Tyskland minskar stödet till solceller," *Ny Teknik*, 2010.
- [6] L. Wissing, "National survey report of pv power applications in germany," tech. rep., BMU – German Federal Ministry for the Environment, Nature Conservation and Nuclear Safety, 2008.
- [7] K. Taretto, U. Rau, and J. Werner, "Numerical simulation of grain boundary effects in cu(in,ga)se₂ thin-film solar cells," *Thin Solid Films*, vol. 480-481, pp. 8–12, 2005.
- [8] P. Würfel, *Physics of Solar Cells*. Wiley-VCH, 2005.
- [9] P. Y. Yu and M. Cardona, *Fundamentals of semiconductors*. Springer, 2001.
- [10] K. L. Chopra, P. D. Paulson, and V. Dutta, "Thin film solar cells: an overview," *Progress in Photovoltaics*, vol. 12, pp. 69–92, 2004.
- [11] V. Fthenakis, "Sustainability of photovoltaics: The case for thin-film solar cells," *Renewable and Sustainable Energy Reviews*, vol. 13, pp. 2746–2750, 2009.
- [12] K. Ramanathan, G. Teeter, J. C. Keane, and R. Noufi, "Properties of high-efficiency cuingase₂ thin film solar cells," *Thin Solid Films*, vol. 480-481, p. 499.502, 2005.
- [13] M. A. Green, K. Emery, Y. Hishikawa, and W. Warta, "Solar cell efficiency tables (version 36)," *Progress in Photovoltaics: Research and applications*, vol. 18, pp. 346–352, 2010.

- [14] H. Zachmann, "Untersuchung der strukturellen und elektrischen schichteigenschaften bei der ionenstrahlgestützten abscheidung von $\text{Cu}(\text{In,Ga})\text{Se}_2$," Master's thesis, Universität Leipzig, 2007.
- [15] A. Virtuani, E. Lotter, M. Powalla, U. Rau, and J. Werner, "Highly resistive $\text{Cu}(\text{In,Ga})\text{Se}_2$ absorbers for improved low-irradiance performance of thin-film solar cells," *Thin Solid Films*, vol. 451-452, pp. 160-165, 2004.
- [16] S. Ishizukaa, K. Sakuraia, A. Yamadaa, K. Matsubaraa, P. Fonsa, K. Iwataa, S. Nakamurab, Y. Kimurab, T. Babab, H. Nakanishib, T. Kojimaa, and S. Nikia, "Fabrication of wide-gap $\text{Cu}(\text{In}_{1-x}, \text{Ga}_x)\text{Se}_2$ thin film solar cells: a study on the correlation of cell performance with highly resistive i-zno layer thickness," *Solar Energy Materials & Solar Cells*, vol. 87, pp. 541-548, 2005.
- [17] U. Rau and M. Schmidt, "Electronic properties of $\text{ZnO}/\text{CdS}/\text{Cu}(\text{In,Ga})\text{Se}_2$ solar cells - aspects of heterojunction formation," *Thin Solid Films*, vol. 387, pp. 141-146, 2001.
- [18] M. F. Stuckings and A. W. Blakers, "A study of shading and resistive loss from the fingers of encapsulated solar cells," *Solar Energy Materials and Solar Cells*, vol. 59, no. 3, pp. 233 - 242, 1999.
- [19] C. Chamberlin, P. Lehman, J. Zoellick, and G. Pauletto, "Effects of mismatch losses in photovoltaic arrays," *Solar Energy*, vol. 54, pp. 165-171, MAR 1995.
- [20] N. Gautam and N. Kaushika, "An efficient algorithm to simulate the electrical performance of solar photovoltaic arrays," *Energy*, vol. 27, pp. 347-361, APR 2002.
- [21] N. Gautam and N. Kaushika, "Reliability evaluation of solar photovoltaic arrays," *Solar Energy*, vol. 72, no. 2, pp. 129-141, 2002.
- [22] Y.-H. Ji, J.-G. Kim, S.-H. Park, J.-H. Kim, and C.-Y. Won, "C-language Based PV Array Simulation Technique Considering Effects of Partial Shading," in *2009 IEEE international conference on industrial technology, vols 1-3*, (345 E 47TH ST, NEW YORK, NY 10017 USA), pp. 1152-1157, IEEE, IEEE, 2009. IEEE International Conference on Industrial Technology, Churchill, AUSTRALIA, FEB 10-13, 2009.
- [23] K. Wilson, D. De Ceuster, and R. A. Sinton, "Measuring the effect of cell mismatch on module output," pp. 916-919, 2006.
- [24] N. Kaushika and A. K. Rai, "An investigation of mismatch losses in solar photovoltaics cell networks," *Energy*, vol. 32, pp. 755-759, 2005.
- [25] P. H. Nguyen, T. Easwarakhanthan, and S. Ravelet, "Influence of parasitic resistances on the mismatch relative power loss of solar cell modules," *Revue Physic Applied*, vol. 20, pp. 689-693, 1985.

- [26] H. Patel and V. Agarwal, "Matlab-based modeling to study the effect of partial shading on pv array characteristics," *IEEE Transactions on Energy Conversion*, vol. 23, no. 1, pp. 302–310, 2008.
- [27] V. Quaschnig and R. Hanitsch, "Numerical simulation of current-voltage characteristics of photovoltaic systems with shaded solar cells," *Solar Energy*, vol. 56, pp. 513–520, JUN 1996.
- [28] X. Yao, J. Li, D. Xia, and Y. Gao, "Research of simulation model for pv array based on matlab," in *Proceedings of first international conference of modelling and simulation, vol iii - modelling and simulation in electronics, computing, and bio-medicine* (Bao, HG and Jiang, Y, ed.), pp. 293–298, 2008.
- [29] G. T., Koishiyev, and J. R. Sites, "Impact of sheet resistance on 2-d modeling of thin-film solar cells," *Solar Energy Materials & Solar Cells*, vol. 93, pp. 350–354, 2009.
- [30] P. O. Grabitz, U. Rau, and J. H. Werner, "Modeling of spatially inhomogeneous solar cells by a multi-diode approach," *Physica Status Solidi A - Applications And Materials Science*, vol. 202, pp. 2920–2927, 2005.
- [31] M. Burgelman, P. Nollet, and S. Degrave, "Modelling polycrystalline semiconductor solar cells," in *Thin Solid Films*, vol. 361, pp. 527–532, February 2000.
- [32] A. Froitzheim, R. Stangl, M. Kriegel, L. Elstner, and W. Fuhs, "Aforshet, a computer program for the simulation of heterojunction solar cells to be distributed for public use," in *Proc. WCPEC-3,,* 2003.
- [33] U. Malm and M. Edoff, "2D device modelling and finite element simulations for thin-film solar cells," *Solar Energy Materials and Solar Cells*, vol. 93, pp. 1066–1069, JUN 2009. 17th International Photovoltaic Science and Engineering Conference, Fukuoka, JAPAN, DEC 03-07, 2007.
- [34] U. Malm and M. Edoff, "Simulating Material Inhomogeneities and Defects in CIGS Thin-film Solar Cells," *Progress in Photovoltaics*, vol. 17, pp. 306–314, AUG 2009.
- [35] R. Brendel, "Modeling solar cells with the dopant-diffused layers treated as conductive boundaries," *Progress in Photovoltaics*, vol. 10, pp. 954–966, 2010.
- [36] A. R. Hambley, *Electronics*. Prentice-Hall, Inc, Upper Saddle River, New Jersey, 2000.
- [37] C. Johnson, *Numerical solution of partial differential equations by the finite element method*. Studentlitteratur, 1987.
- [38] J. M. Thijssen, *Computational physics*. Cambridge University Press, second ed., 2007.
- [39] R. W. Pryor, *Multiphysics modeling using COMSOL: A first principles approach*. Jones and Bartlett Publishers, 2011.

- [40] U. Rau, P. O. Grabitz, and J. H. Werner, "Resistive limitations to spatially inhomogeneous electronic losses in solar cells," *Applied Physics Letters*, vol. 85, pp. 6010–6012, 2004.